

www.acsami.org Research Article

Photodynamic Coatings on Polymer Microfibers for Pathogen Inactivation: Effects of Application Method and Composition

Bharadwaja S. T. Peddinti, Nicolas Morales-Gagnon, Behnam Pourdeyhimi, Frank Scholle, Richard J. Spontak,* and Reza A. Ghiladi*



Cite This: ACS Appl. Mater. Interfaces 2021, 13, 155–163

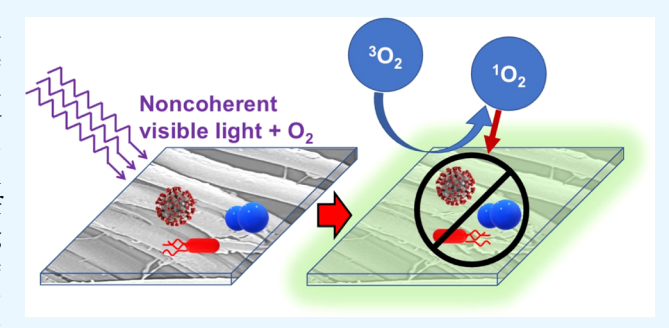


ACCESS

Metrics & More

Article Recommendations

ABSTRACT: A substantial increase in the risk of hospital-acquired infections (HAIs) has greatly impacted the global healthcare industry. Harmful pathogens adhere to a variety of surfaces and infect personnel on contact, thereby promoting transmission to new hosts. This is particularly worrisome in the case of antibiotic-resistant pathogens, which constitute a growing threat to human health worldwide and require new preventative routes of disinfection. In this study, we have incorporated different loading levels of a porphyrin photosensitizer capable of generating reactive singlet oxygen in the presence of O_2 and visible light in a water-soluble, photo-cross-linkable polymer coating, which was sub-



sequently deposited on polymer microfibers. Two different application methods are considered, and the morphological and chemical characteristics of these coated fibers are analyzed to detect the presence of the coating and photosensitizer. To discern the efficacy of the fibers against pathogenic bacteria, photodynamic inactivation has been performed on two different bacterial strains, *Staphylococcus aureus* and antibiotic-resistant *Escherichia coli*, with population reductions of >99.9999 and 99.6%, respectively, after exposure to visible light for 1 h. In response to the current COVID-19 pandemic, we also confirm that these coated fibers can inactivate a human common cold coronavirus serving as a surrogate for the SARS-CoV-2 virus.

KEYWORDS: hospital-acquired infections, photodynamic coatings, porphyrin photosensitizer, SARS-CoV-2 virus, polymer microfibers

■ INTRODUCTION

Hospital-acquired infections (HAIs) are rapidly becoming a major threat to global health care. In these and related instances, pathogens adhere to common surfaces and are able to survive for extended periods of time or proliferate, thereby creating a risk of transmission via fomites.² On average, ~5% of hospitalized patients acquire HAIs, as reported³ by the U.S. Centers for Disease Control and Prevention (CDC). Although primarily affecting people suffering from compromised immune systems, even relatively healthy patients are susceptible to such infections. This statistic translates to ~100 000 deaths annually in the United States alone. Of growing concern in this vein are antibiotic-resistant pathogens (ARPs). Improper use or unnecessary prescription of antibiotics, coupled with the introduction of antibiotics in the food chain, has promoted a dramatic and worrisome increase in ARPs. Examples of superbugs (urgent and serious threats as per CDC classification or, as the media has coined,5 "nightmare bacteria") that are resistant to last-resort antibiotics include methicillin-resistant Staphylococcus aureus (MRSA), vancomycin-resistant Enterococcus faecium (VRE), and multidrug-resistant Escherichia coli (e.g., strain ST131) bacteria. According to the CDC, more than 2.8 million infections result

each year due in the U.S. to ARP-related infections, leading to ~49 000 deaths. A recent survey predicts⁷ that global infections caused by ARPs will increase drastically to ~10 million deaths annually, thereby surpassing all cancer-related deaths, by 2050. In addition, the annual expenditure invested in the treatment of these potentially fatal infections is estimated to be \$28–45 billion. While ARPs are limited to bacteria and fungi, viruses such as influenza A and B (which are responsible for epidemics every year), human adenovirus, and pathogenic coronaviruses (e.g., SARS-CoV and MERS-CoV¹⁰) further contribute to the expanding HAI health crisis.

To combat this escalating threat, alternate routes of effective antimicrobial inactivation on various substrates must be identified and commercialized soon to prevent needless loss of life, as well as reduce the financial strain on the healthcare sector. Today, polymeric surfaces constitute one of the most

Received: September 24, 2020 Accepted: November 25, 2020 Published: December 23, 2020





ubiquitous substrates encountered in daily life. For this reason, we exclusively consider polymer fibers in this study since they account for a wide range of textile products used worldwide. While various chemical and radiative methodologies are routinely employed to kill surface microbes, they often require labor-intensive application and strict adherence to protocols, harm mammalian cells, contaminate the environment, and remain temporary solutions (i.e., they do not prevent recontamination). Strategies developed to endow thermoplastic and elastomeric substrates with self-sterilizing antimicrobial properties rely extensively on either (i) surface or bulk incorporation of metal (e.g., Ag¹³ or Cu¹⁴) or metal oxide (e.g., TiO₂¹⁵) nanoparticles or (ii) surface-grafted or -grown organic building blocks that contain inherently antimicrobial moieties such as quaternary ammonium compounds (QACs)¹⁶ or quaternary phosphonium compounds (QPCs).¹⁷ In the specific case of bacteria, however, these pathogens can become resistant to the toxicity of metal nanoparticles, 18 which can likewise leach into the environment and introduce new health challenges associated with the food chain.¹⁹ Similarly, quaternized compounds can have an adverse impact on the environment.²⁰ Moreover, metal (oxide) and cationic compounds that kill bacteria through cell disruption or lysis of the negatively charged cell membrane by electrostatic interaction²¹ are generally ineffective against non-enveloped viruses, although enveloped viruses containing a phospholipid membrane can be inactivated. The critical question we pose here is as follows: can a facile and broad-spectrum disinfection alternative be developed that is preventative, eco-friendly, and compatible with the textile sector?

Recently, we have demonstrated two material designs that indicate such alternatives are indeed possible. One design derives from a partially sulfonated (anionic) multiblock polymer that, in the presence of water, drastically lowers the surface pH below what is tolerable by many pathogens, thereby killing a wide range of bacteria and viruses to the minimum detection limit (MDL) of 99.9999% in just minutes with no additional stimuli.²² Recent studies²³ confirm that this approach is equally effective against the SARS-CoV-2 virus responsible for the COVID-19 pandemic that has reportedly infected nearly 25 million people, claiming the lives of over 840 000 around the world²⁴ as of the time of this writing. Although this revolutionary approach is promising, further studies are necessary to functionalize the various polymers used in the textile industry. The second material design involves the surface attachment^{25,26} or bulk incorporation²⁷ of photosensitizer (PS) molecules that activate upon exposure to incoherent visible light and generate cytotoxic singlet oxygen (¹O₂) from ground-state oxygen. Singlet oxygen nonspecifically reacts with multiple chemical constituents of microbial membranes to induce inactivation,²⁸ in which case even drug-resistant microbes are susceptible with little to no chance of developing resistance. Due to the relatively short lifetime of $^{1}O_{2}$ (reported²⁹ as $\sim 2 \mu s$ in air), however, the distance from a surface over which ¹O₂ remains antimicrobial is typically just a few hundred nanometers in solution. Previously, we have demonstrated³⁰ that the addition of a porphyrin PS to a highly nonpolar block copolyolefin prepared by solution casting, followed by repeated melt pressing, yielded encouraging broadspectrum antimicrobial properties (>99.89% mortality) against not only the same bacteria and viruses tested in our charged multiblock copolymer study²² but also fungi.³¹

Here, we extend the concept of photodynamic polymers to photodynamic polymer coatings by incorporating the same PS into a photo-cross-linkable polymer that is water-soluble to avoid the need for volatile organic compounds (VOCs) during deposition. Of particular interest here are coatings on fibrous polymer substrates since polymer fibers are representative of personal protection equipment (PPE) and they afford more surface area than films, thereby increasing PS/pathogen interactions. The photo-cross-linking behavior of the coating utilized in this work has been previously investigated,³² as have the polymer fibers that constitute example substrates.³³ As we have already established the broad-spectrum efficacy of the PS with regard to its ability to inactivate a wide range of bacterial strains, we have elected to monitor just two representative bacteria, one Gram positive and one Gram negative, for proof of concept in the present antimicrobial photodynamic inactivation (aPDI) study. In response to the ongoing COVID-19 pandemic, we likewise examine the inactivation of a human coronavirus (HCoV229E) that serves³⁴ as a less pathogenic proxy for the SARS-CoV-2 virus.

■ EXPERIMENTAL SECTION

Materials. The PS employed here was zinc tetra(4-N-methylpyridyl)porphine (ZnTMPyP $^{4+}$) tetrachloride, the chemical structure of which is provided in Scheme 1. It was obtained from

Scheme 1. Chemical Structures of the Zinc Tetra(4-N-methylpyridyl)porphine (ZnTMPyP⁴⁺) Photosensitizer (*Left*) and the Water-Soluble N-Methyl-4(4'-formylstyryl)pyridinium Methosulfate Acetal Poly(vinyl alcohol) (SbQ-PVA) Photo-Cross-Linkable Coating (*Right*) Employed in the Present Study^a

^aThe counterion on ZnTMPyP⁴⁺ is Cl⁻.

Frontier Scientific (Logan, UT). The UV-cross-linkable coating, Nmethyl-4(4'-formylstyryl)pyridinium methosulfate acetal poly(vinyl alcohol) (SbQ-PVA) with 4.1 mol % functional SbQ groups, was purchased from Polysciences, Inc. (Warrington, PA) and is included in Scheme 1. Bicomponent fibers composed of nylon-6 (PA6; BASF B27E) "islands" embedded in a poly(lactic acid) (PLA; Natureworks 6202D) "sea" were produced in an "island-in-the-sea" cross-sectional arrangement³⁵ (with 37 PA6 channels in a PLA matrix). Spunbond fabrics composed of the bicomponent PA6/PLA fibers were formed on a Reicofil R4s Spunbond line (1.2 m wide) and bonded in an Andritz hydroentangling unit, equipped with a prewet station and seven injectors capable of pressures up to 250 bar, at the Nonwovens Institute located at the North Carolina State University. Water jet pressures used during hydroentangling were ramped from 30 to 225 bar. The PLA matrix was removed chemically in a Jet Dyeing instrument (typically used for dyeing but likewise ideal for PLA removal because of the constant agitation) to release the PA6 microfibers after hydroentangling. Operating parameters included the following: 6-20 L liquor, 0.1-1.5 kg fibers, 4-30 m/min agitation speed, 20-150 °C (at 4 bar), and a heating rate of 2-4 °C/min. The aqueous liquor contained 8% NaOH, which readily removes PLA at 80 °C, and the resultant PA6 microfiber mats were coated as produced. Buffer salts were procured from Fischer Scientific (Pittsburgh, PA), whereas tryptic soy broth (TSB) and Miller lysogenic broth (LB) were obtained from Teknova (Hollister, CA) and EMD Chemicals (Billerica, MA), respectively. All media and buffer solutions were prepared in deionized (DI) water.

Methods. Coating Protocols. After square sections measuring 5 cm × 5 cm and weighing ~200 mg were cut from the PA6 mat, SbQ-PVA was dissolved in DI water and stirred for 15 min at ambient temperature until full dissolution was achieved according to the unaided eye. For spray-coated (SCPA6) fibers, ZnTMPyP⁴⁺ powder was added at three different PS loading levels (0.01, 0.1, and 1.0% w/ w ZnTMPyP4+/SbQ-PVA) to aqueous SbQ-PVA solutions at a constant concentration of 10% w/v SbQ-PVA/water. For dip-coated (DCPA6) fibers, the loading level was held constant at 10% w/w ZnTMPyP4+/SbQ-PVA, but the solution concentration was varied from 0.01 to 1.0% w/v (ZnTMPyP4+ + SbQ-PVA)/water to alter the coating thickness. In both cases, the ternary solutions were subsequently stirred for an additional 15 min prior to coating. Each of the SCPA6 fibers was coated with ~2 mL of solution from a multipurpose precision airbrush with a 0.3 mm fluid tip, whereas the DCPA6 fibers were produced by manual dipping into the above solutions. All specimens were cured under UV light at 36 W for 1 h and then immersed in the parent aqueous SbQ-PVA solution (to add a capping layer) prior to final drying and UV curing for an additional 1 h. Two points warrant particular mention here: initial immersion of the coated fibers into aqueous SbQ-PVA solutions likely extracted some of the PS, resulting in marginally lower concentrations than the original targets, and the PS-free capping layer further decreased the extraction of ZnTMPyP⁴⁺. After this last step, all specimens were washed overnight to remove unbound porphyrin to mitigate leaching during aPDI analysis. This protocol was similar to that previously reported.^{25–27,30} The specimens were thoroughly dried prior to exposure to bacteria.

Fiber Characterization. The morphologies of the bicomponent PA6/PLA, neat PA6, and coated PA6 fibers were examined by scanning electron microscopy (SEM) performed in a variable-pressure Hitachi S3200N microscope equipped with an Oxford energydispersive X-ray spectroscopy (EDS) detector. The fiber mats were mounted on aluminum stubs with carbon tape and sputtered with ~35 nm of Au-Pd to reduce charging. Images and EDS spectra were acquired at an accelerating voltage of 20 kV and a column pressure of 30 Pa (N2). Time-of-flight secondary ion mass spectroscopy (ToF-SIMS) analysis was conducted on neat and coated PA6 fibers in an IONTOF ToF-SIMS V instrument equipped with a 25 kV bismuth ion (Bi+) sputtering gun. High-resolution ion-specific images were collected wherein the chlorine counterion (Cl-) on ZnTMPyP4+ served to indicate the presence of the PS. Neat and coated PA6 fibers were also subjected to X-ray photoelectron spectroscopy (XPS) performed on a PHOIBOS 150 spectrometer operated at 10-14 kV. The nitrogen (N) content and oxygen/carbon (O/C) ratio were analyzed to ascertain the coverage of the SbQ-PVA coatings.

Antimicrobial Analysis. The aPDI studies were performed on two bacterial strains that promote nosocomial infections: methicillinsusceptible Staphylococcus aureus 29213 (MSSA), an example of Gram-positive bacteria, and ampicillin-resistant Escherichia coli (AREC), an example of Gram-negative bacteria. While MSSA was cultured without antibiotics in TSB, AREC BL21-(De3)pLysS (Stratagene, San Diego, CA) was cultured in LB containing 100 μ g/mL ampicillin. In each case, 5 mL of broth was used to grow each bacterial strain in a culture tube incubated at 37 °C in an orbital shaker operated at 250 rpm. A Genesys 10 UV scanning spectrophotometer operated at a wavelength of 600 nm measured the optical density (OD) of each bacterial broth. Both strains were grown to broth concentrations possessing an OD of ~0.4, which corresponds to a bacterial concentration of $(1-4) \times 10^8$ CFU/mL (where CFU denotes colony-forming unit). Afterward, the broths were centrifuged for 5 min at 3600 rpm, and the supernatant was subsequently discarded. Resultant bacterial pellets produced in this

fashion were resuspended in 5 mL of phosphate-buffered saline (PBS) solution prior to aPDI analysis of the SCPA6- and DCPA6-coated fibers. This analysis required that the coated fiber mats were cut with a hole punch into discs, each measuring \sim 1.5 cm in diameter so that it could fit precisely in the bottom of a well in a 24-well plate. After all of the discs were inserted into the wells, 200 μ L of bacterial solution was pipetted from each PBS stock solution and uniformly deposited on top of each disc. The HCoV229E virus was grown on the human hepatocarcinoma cell line (Huh-7) in cell growth media (DMEM, 1% antibiotics, 10% fetal bovine serum, FBS) at 33 °C. In this case, fibrous mats were cut to precisely fit the well bottoms of a 96-well plate, and 25 μ L of virus suspension was added to the plates for a given exposure time.

All aPDI analyses were performed under ambient conditions via illumination provided by a LumaCare LC-122 incoherent visible light source. The lamp was equipped with an OSRAM 64653 HLX Xenophot bulb (250 W, 24 V) and employed an LUM V fiber-optic probe (400-700 nm band-pass filter) with a 95 \pm 3% average transmittance. An Orphir Optronics Ltd. Orion power meter measured the fluence rate of the light source. In accord with our previous studies, ³⁰ illumination intensities of 65 ± 5 and 80 ± 5 mW/ cm² were employed in aPDI studies of MSSA and AREC, respectively. In the case of the HCoV229E virus, both light intensities were employed to induce aPDI. After the introduction of microbial suspension, the disc-containing wells were covered with Al foil and stored in the dark for 60 min for two purposes: (1) the results served as a dark control for aPDI and (2) the results would reveal if either substrate or ZnTMPyP⁴⁺ possessed inherent toxicity in the absence of light. For the bacterial tests, well plates containing only suspension without a substrate served as a reference used to calculate the inactivation for other control and illuminated specimens. Following illumination under the above conditions, the discs were removed and placed in a 15 mL centrifuge tube, and the bottom of each well was washed with 5 mL of PBS and then added to the centrifuge tube containing the disc. The tube was vortexed thoroughly to resuspend the adhered bacteria.

After the discs were removed, the resulting suspension was centrifuged at 3600 rpm for 5 min. The supernatant was discarded, and the bacterial pellet was resuspended by vortexing in 200 μL of PBS. Then, 40 µL of bacterial suspension was withdrawn and added to 360 μ L of PBS in an aliquot. This procedure was repeated five times to generate six serial dilutions of each illuminated specimen. Finally, 10 μ L was pipetted from each aliquot and placed on sixcolumn-square plates that were previously prepared with agar and antibiotic-free broth for both bacteria. The agar plates were stored overnight in an oven maintained at 37 °C. The same procedure was followed for specimens kept in the dark. Colony-forming units were later counted, and the corresponding bacterial inactivation level (along with the *p*-value from a student statistical *t*-test) was calculated. After exposure of the HCoV229E virus to illumination for 60 min, 75 μL of infection media (MEM 1% antibiotics, 1% FBS, 1% HEPES buffer) was added, and the virus was eluted by triturating several times, followed by rapid transfer to new wells. Virus suspensions were immediately diluted serially 10-fold, and six replicates of each dilution were used to infect Huh-7 cells seeded the previous day at a density of 10^4 cells per well in a TCID₅₀ assay protocol. After 2 h, 50 μ L of cell growth media was added and the plates were incubated at 33 °C with 5% CO₂. After 96 h, the cytopathic effect was quantitated by visual inspection, and resulting TCID₅₀/mL values were calculated according to the Spearman-Kaerber method. 36,3

■ RESULTS AND DISCUSSION

Fiber Characteristics. The method for producing relatively uniform PA6 microfibers for use in this study requires bicomponent fiber spinning wherein PA6 is dispersed within a PLA matrix. Such fiber spinning can exploit a wide range of cross-sectional geometries, but one that is used to recover a large population of microfibers for nonwoven mats is the "island-in-a-sea" configuration. ³⁵ In the present study, 37

equally sized/spaced PA6 islands are arranged in a continuous PLA matrix. Cross-sectional SEM images of such bicomponent fibers are presented elsewhere 33 and are not reproduced here. Since the PLA is a hydrolyzable polyester whereas PA6 is highly resistant to dilute alkaline solutions, the PLA can be selectively removed by exposure to NaOH(aq), thereby leaving behind discrete PA6 microfibers measuring about 2–3 μm across, according to SEM images such as that displayed in Figure 1. The series of SEM images provided in Figure 2

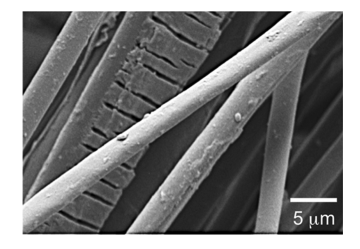


Figure 1. SEM image of unmodified PA6 microfibers recovered upon removal of the PLA matrix in bicomponent PA6/PLA "island-in-the-sea" fibers, followed by hydroentanglement to form a nonwoven mat.

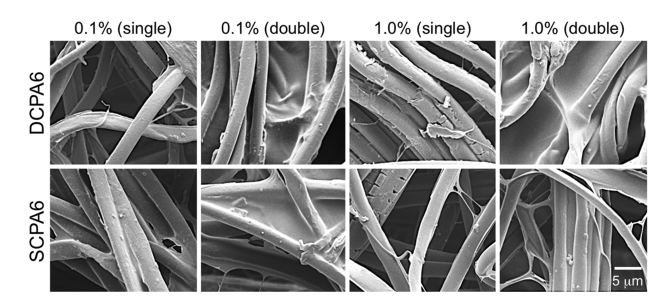


Figure 2. SEM images acquired from DCPA6 (top row) and SCPA6 (bottom row) fibers coated with SbQ-PVA + ZnTMPyP⁴⁺ at different coating concentrations (DCPA6), PS loading levels (SCPA6), and coating layers (labeled along the top).

confirms the existence of a SbQ-PVA coating on SCPA6 and DCPA6 fibers, and the average coating thickness is estimated to be \sim 150–200 nm on SCPA6 fibers. Neither coating process appears to be particularly efficient, as indicated by the formation of cross-linked SbQ-PVA webs and sheets located between, and thus connecting, adjacent fibers. This feature is particularly evident when a second SbQ-PVA coating is applied. The extent to which the PA6 is coated can also be gleaned from XPS spectra (cf. Figure 3). As seen from the extracted elemental compositions listed in Table 1, addition of the SbQ-PVA coating is signified by an increase in surface O and a reduction in N (from PA6). In fact, the surface N content of the SCPA6 specimen is below the detection limit, which implies that the PA6 fiber is largely, if not completely, unexposed, whereas the DCPA6 specimen exhibits a detectable N level corresponding to either very thin or only partial fiber coverage. Moreover, the O/C ratios of the two coated specimens are quantitatively similar, whereas that for neat PA6 is noticeably lower. These conclusions are further corroborated by $\stackrel{\cdot}{EDS}$ in which Cl from the counterion on ZnTMPyP⁴⁺ (see Scheme 1) is used to monitor the PS loading level (see Table 2).

Another method by which to visualize the extent to which the PA6 microfibers are coated with ZnTMPyP⁴⁺-containing SbQ-PVA involves ToF-SIMS imaging. Here, three ionic species are of particular interest: CNO⁻ from neat PA6,

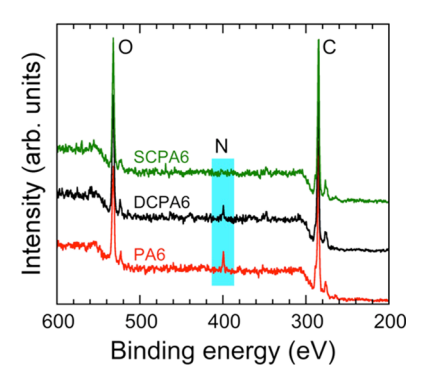


Figure 3. XPS spectra collected from PA6, as well as DCPA6 (1.0% w/v) and SCPA6 (1.0% w/w), fibers (labeled and color-coded) with relevant elemental binding energies identified. The shaded area highlights the binding energy for nitrogen.

Table 1. Surface Composition Results of Neat and Coated Microfibers According to XPS Analysis

specimen	C (atom %)	O (atom %)	N (atom %)	O/C		
PA6	75.2	20.6	4.2	0.27		
DCPA6 (1.0% w/v)	75.1	21.7	1.9	0.29		
SCPA6 (1.0% w/w)	76.1	23.2	0.0 ^a	0.30		
^a Below the detection limit.						

Table 2. Bulk Composition Results of Neat and Coated Microfibers According to EDS Analysis

specimen	C (wt %)	O (wt %)	Cl (wt %)
PA6	72.8	24.9	0.0
DCPA6 (0.1% w/v)	77.2	19.4	1.2
DCPA6 (1.0% w/v)	75.1	20.3	2.4
SCPA6 (0.1% w/w)	71.0	18.9	1.8
SCPA6 (1.0% w/w)	71.9	17.7	3.4

C₂H₃O₂⁻ from SbQ-PVA, and Cl⁻ from ZnTMPyP⁴⁺. Images acquired from each of these species are presented for neat PA6, DCPA6, and SCPA6 specimens in Figures 4–6 and reveal

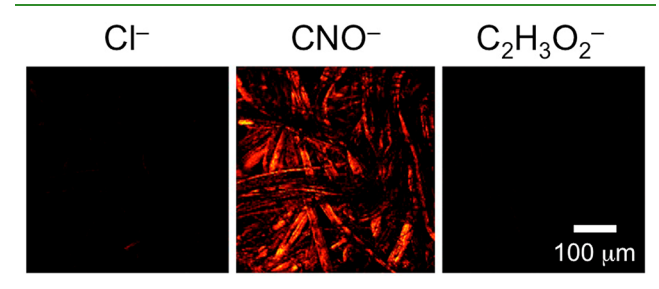


Figure 4. ToF-SIMS images of Cl $^-$ (the PS counterion), CNO $^-$ (the PA6 substrate), and $C_2H_3O_2^-$ (the SbQ-PVA coating) acquired from neat PA6 microfibers.

several noteworthy features. In the case of unmodified PA6 (Figure 4), only CNO $^-$ ions from the neat fibers are sufficiently detectable at the acquisition conditions employed to generate an image. This confirms that the fibers are uncoated. Images of the DCPA6 specimens in Figure 5 at different coating concentrations (coating thicknesses) indicate the presence of both CNO $^-$ and $C_2H_3O_2^-$ ions, verifying the presence of the SbQ-PVA coating. As the coating concentration is increased, the intensity of the CNO $^-$ images systematically decreases, while that of the $C_2H_3O_2^-$ images

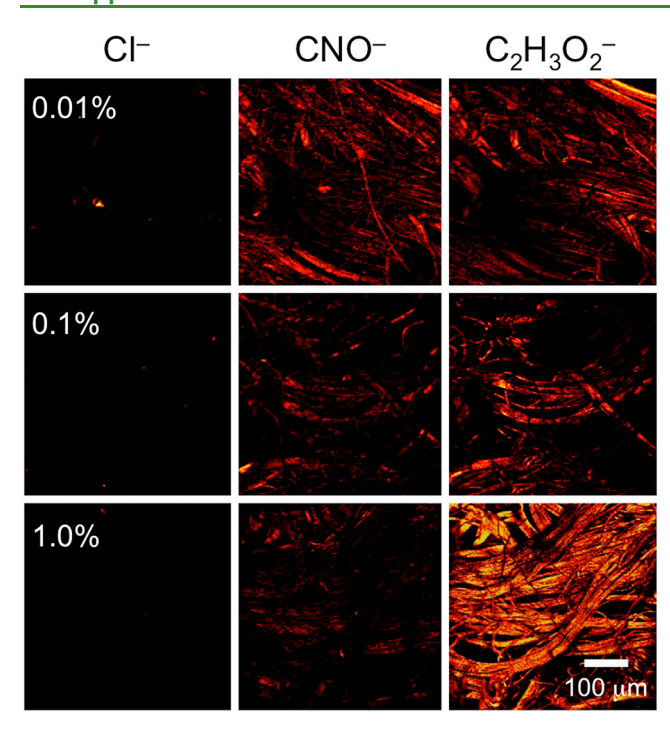


Figure 5. ToF-SIMS images of Cl⁻ (the PS counterion), CNO⁻ (the PA6 substrate), and $C_2H_3O_2^-$ (the SbQ-PVA coating) acquired from DCPA6-coated fibers at different coating concentrations (labeled).

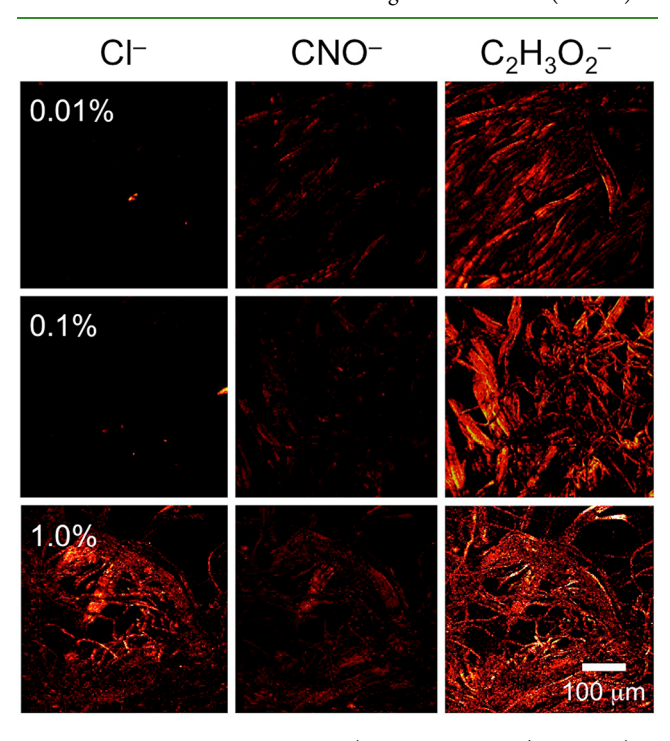


Figure 6. ToF-SIMS images of Cl $^-$ (the PS counterion), CNO $^-$ (the PA6 substrate), and $C_2H_3O_2^-$ (the SbQ-PVA coating) acquired from SCPA6-coated fibers at different coating concentrations (labeled).

conversely increases, implying that the fibers become increasingly better coated. Several isolated bright spots in the Cl⁻ images likewise establish the existence of the ZnTMPyP⁴⁺ PS, most likely in the form of discrete aggregates. Qualitatively similar results are observed for the SCPA6 specimens in Figure 6 with two notable exceptions. The CNO⁻ images corresponding to PA6 are significantly less well defined and

intense, which suggests that the SCPA6 fibers are more consistently coated with SbQ-PVA than the analogous DCPA6 ones, in agreement with our XPS findings. The second difference is that the Cl⁻ image collected from the SCPA6 specimen at a 1 wt % PS loading level (relative to the coating) displays continuous regions that indicate the ZnTMPyP⁴⁺ PS is located throughout the coated fibers within these regions. Taken together, these results suggest that the coatings on the SCPA6 fibers should be more effective at aPDI than their DCPA6 counterparts.

aPDI Analysis. Due to the difference in the structure of Gram-positive and Gram-negative bacteria, two different illumination intensities (65 \pm 5 and 80 \pm 5 mW/cm², respectively) have been utilized in this aPDI study. Gramnegative bacteria possess an extra layer of outer membrane in addition to the plasma membrane and peptidoglycan layer that together protect the intracellular components of Gram-positive bacteria. The peptidoglycan layer, mainly composed of sugars and amino acids, is relatively easy to disrupt, which subsequently leads to cell wall lysis and leakage of intracellular components from Gram-positive bacteria. The extra layer of outer membrane in Gram-negative bacteria, on the other hand, impedes efforts to destroy the cell wall, thereby sheltering the intracellular components. For this reason, a higher light intensity is required against Gram-negative AREC to produce more ¹O₂ and induce cell wall disruption. Another important consideration in the present study is fiber coating uniformity, which is expected to influence the antibacterial performance of the SCPA6 and DCPA6 fibers. This difference, as well as the role of coating concentration, is apparent in Figure 7 for coated

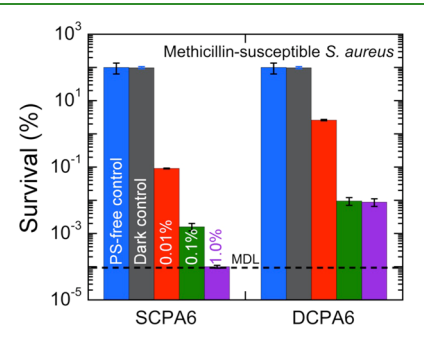


Figure 7. MSSA survival after aPDI in the presence of SCPA6- and DCPA6-coated fibers for 1 h at a light intensity of $65 \pm 5 \text{ mW/cm}^2$. The controls and PS loading levels (SCPA6) or solution concentrations (DCPA6) are labeled and color-coded. The error bars correspond to the standard error.

fibers exposed to MSSA bacteria. While both types of coated fibers unequivocally display evidence of antibacterial effectiveness, the SCPA6 fibers tend to outperform their DCPA6 analogues at the same coating concentration even though the DCPA6 fibers possess a higher ZnTMPyP⁴⁺ PS level. In the case of SCPA6 specimens, an increase in ZnTMPyP⁴⁺ loading promotes improved antibacterial performance, eventually reaching the MDL (99.9999% inactivation, with a 6 log unit reduction in CFU/mL and a *p*-value <0.0001) at the highest level tested. The efficacy of the DCPA6 fibers with regard to MSSA inactivation in Figure 7, as well as for AREC inactivation in Figure 8, is, however, generally less pronounced than the SCPA6 fibers and, in the specific case of MSSA, appears to become independent of solution concentration (*i.e.*, coating thickness). It is important to remember that both

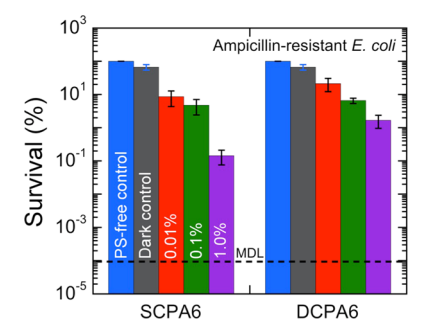


Figure 8. AREC survival after aPDI in the presence of SCPA6- and DCPA6-coated fibers for 1 h at a light intensity of $80 \pm 5 \text{ mW/cm}^2$. The controls and PS loading levels (SCPA6) or solution concentrations (DCPA6) are labeled and color-coded. The error bars correspond to the standard error.

series of coated fibers contain a second coating of ZnTMPyP⁴⁺-free SbQ-PVA, which serves as a capping layer to prevent ZnTMPyP⁴⁺ leaching during the aPDI tests. Upon illumination, any ¹O₂ generated by the ZnTMPyP⁴⁺ PS in the active coating layer must diffuse through the capping layer to ultimately affect bacteria. This consideration, coupled with thinner and possibly less uniform coatings on the DCPA6 fibers, most likely constitutes the reason for the lower efficacy of the DCPA6 fibers relative to the SCPA6 fibers despite the higher ZnTMPyP⁴⁺ loading level in the DCPA6 fibers.

To compare the results from the coated fibers developed here against our previously reported results wherein the PS is embedded in a nonpolar block copolyolefin matrix,³⁰ the individual results displayed in Figures 7 and 8 are combined with those earlier findings in Figure 9 to elucidate the efficacy

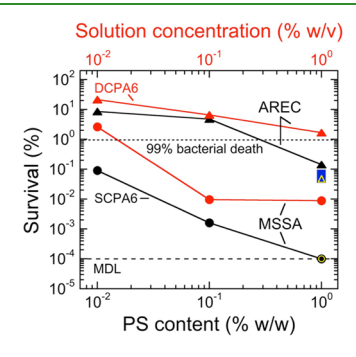


Figure 9. MSSA (filled circles) and AREC (filled triangles) survival on SCPA6- (black, bottom abscissa axis) and DCPA6- (red, top abscissa axis) coated fibers as measured in Figures 7 and 8, respectively. The solid lines serve to connect the data, whereas the dashed and dotted lines identify the MDL and 99% death conditions, respectively. All of these results are statistically significant with *p*-values below 0.0236. Included for comparison are results obtained earlier for the same PS embedded at 1.0 wt % in a block copolyolefin matrix (open yellow symbols). The blue shaded region indicates the survival range for all of the Gram-negative bacteria reported elsewhere, ³⁰ whereas all of the Gram-positive bacteria in the same study achieve the MDL, after comparable exposure conditions.

of the incorporation protocols as a function of PS loading level. As expected from the discussion above, we anticipate that the antimicrobial performance will be more pronounced for the Gram-positive (MSSA) bacterial strain than for the Gramnegative (AREC) strain. Our prior study has demonstrated that reduction levels of at least 99.89% can be achieved for

several Gram-negative strains, including AREC, Acinetobacter baumannii and Klebsiella pneumoniae, under the same exposure conditions. This series of bacterial strains is especially relevant here since these pathogens are resistant to various traditional and contemporary pharmaceuticals, 38-43 largely comprising the ESKAPE series (i.e., E. faecium, S. aureus, K. pneumoniae, A. baumannii, Pseudomonas aeruginosa, and Enterobacter species) of bacteria primarily responsible for HAIs,⁴⁴ and they can likewise cause other infectious outbreaks (e.g., food contamination^{45,46}). For AREC, in particular, bulk-functionalized polymer films yield 99.95% inactivation, 30 which is comparable to the best result achieved here (99.86% for the SCPA6 fibers at a 1 wt % PS loading level). In marked contrast, Grampositive bacteria such as MRSA, MSSA, and VRE are much more susceptible to aPDI, previously attaining the MDL (at 99.999% inactivation) under identical exposure conditions. Here, the maximum inactivation levels are 99.9999 and 99.99% for the SCPA6- and DCPA6-coated fibers, respectively, at a 1 wt % PS loading level. As our prior study clearly indicated, however, the level of bacterial inactivation achieved is sensitively dependent on the coupling between light intensity and exposure time.

While the primary intention of this study has been to focus on the antibacterial efficacy of PS-containing coatings on polymer fibers, the need for effective, long-lasting, and comprehensive antimicrobial coatings on PPE around the globe is evident in the present COVID-19 pandemic. This need is particularly urgent since recent studies⁴⁷⁻⁴⁹ have established that the SARS-CoV-2 virus can survive for several days on plastic substrates, including nonwoven fibrous facemasks, and can thus be transmitted by direct contact, in addition to water droplets and aerosols dispersed in the air. 50 Due to its infectivity and facile transmission, the SARS-CoV-2 virus requires Biosafety Level 3 containment, which was not readily attainable for this study. For this reason, we have chosen to examine the HCoV229E virus as a less pathogenic surrogate that has been shown to possess similar environmental stability as the more pathogenic coronaviruses (SARS-CoV, MERS-CoV, and SARS-CoV-2).34 In addition, clinical disinfection protocols are common among all coronaviruses. On the basis of our parallel pH-drop inactivation strategy, we have observed²³ that the HCoV229E virus is more resistant to a precipitous reduction in surface pH than the SARS-CoV-2 virus, although both viruses are completely inactivated (to the MDL) in a significantly shorter exposure time (5-20 min)relative to more traditional antimicrobial surfaces such as copper. 47 The aPDI results obtained here for HCoV229E are presented in Figure 10 and reveal that the uncoated microfibers have little, if any, effect on the virus within experimental uncertainty. In contrast, microfibers subjected to a PS-containing spray coating (1 wt % PS) reveal a substantial reduction in virus survivability after exposure to light at an intensity of 65 mW/cm² for 60 min. In this case, the level of inactivation is 99.7%. By increasing the light intensity to 80 mW/cm² for the same exposure time, the inactivation level is dramatically increased to 99.9998% (corresponding to the MDL), which is comparable to the antibacterial effectiveness measured here. These results are extremely promising, indicating that the aPDI approach can be applied (in the form of a coating) directly to polymer fibers used in PPE, as well as in fibrous furnishings found in homes, offices, temporary housing, and medical facilities.

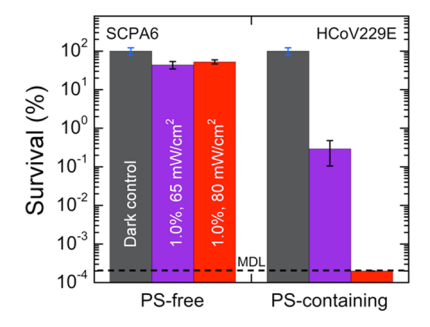


Figure 10. HCoV229E survival after aPDI in the presence of SCPA6-coated fibers for 1 h at two different exposure conditions. The controls, PS loading levels, and light intensities are labeled and color-coded. The error bars correspond to the standard error.

CONCLUSIONS

Photodynamic polymer coatings have been prepared by incorporating a ZnTMPyP4+ PS in UV-cross-linkable SbQ-PVA, followed by deposition, using two different approaches, on microfibers of a common thermoplastic (nylon-6) in the textile industry. An important consideration here is that these coatings are anticipated to remain fully antimicrobial (i.e., capable of producing ¹O₂ in the presence of visible light and atmospheric O₂) insofar as the integrity of the coating is not compromised by factors such as mechanical abrasion/cracking or photobleaching due to long-term activation of the PS. Even if the coatings become damaged, the underlying fibers can readily be recoated using the methodologies reported here. According to SEM analysis, the present microfibers are coated and, depending on the concentration of the coating solution and the number of coatings applied, sheets connecting adjacent fibers are also present. The coverage of coatings prepared by spray deposition is particularly encouraging since corresponding XPS spectra display no signal from nitrogen, which is a characteristic signature of the nylon-6 substrate. These spectra likewise corroborate that the surface oxygen/carbon ratio of fibers coated by either dip or spray deposition increases to a constant level exceeding that of the substrate. Ion-specific images acquired by ToF-SIMS further corroborate these independent results by identifying the presence of C₂H₃O₂⁻ from SbQ-PVA and Cl⁻ (the counterion) from ZnTMPyP⁴⁺ on both types of coated fibers.

Antimicrobial photodynamic inactivation studies conducted against Gram-positive and Gram-negative bacterial strains indicate that, despite deposition-related variations in coating coverage, all of the coated fibers examined here are antibacterial. In fact, a maximum of 99.9999% inactivation (at the MDL) is achieved with methicillin-susceptible *S. aureus*, whereas 99.86% inactivation is observed with ampicillinresistant E. coli. While these results compare favorably with our previous study³⁰ of the same PS in a nonpolar copolyolefin, we note that considerable inactivation (78.57-99.91%) occurs with these coatings at a significantly (100×) lower ZnTMPyP⁴⁺ concentration. With this substantial reduction in PS loading and the use of polymer fibers in conjunction with an eco-friendly water-borne coating, we have demonstrated an economically viable and process-friendly alternative by which to produce anti-infective materials that show promise in the healthcare, agricultural, defense, textile, and food packaging industries. Moreover, although only two bacterial strains have been investigated in this study, we expect on the basis of our consistent findings here (cf. Figure 9) that our previous

successes with other bacteria (*e.g.*, MRSA), as well as (un)encapsulated viruses³⁰ and fungi,³¹ will translate to these coated fibers. In this spirit, we also report that the inactivation of a human coronavirus serving as a surrogate for the SARS-CoV-2 virus³⁴ can reach 99.9998%, thereby confirming that PS-containing coatings can be used in conjunction with PPE to help prevent the spread of COVID-19.

AUTHOR INFORMATION

Corresponding Authors

Richard J. Spontak — Department of Chemical & Biomolecular Engineering, Department of Materials Science & Engineering, and Center for Advanced Virus Experimentation, North Carolina State University, Raleigh, North Carolina 27695, United States; orcid.org/0000-0001-8458-0038; Email: rich spontak@ncsu.edu

Reza A. Ghiladi — Center for Advanced Virus Experimentation and Department of Chemistry, North Carolina State University, Raleigh, North Carolina 27695, United States; Email: reza ghiladi@ncsu.edu

Authors

Bharadwaja S. T. Peddinti – Department of Chemical & Biomolecular Engineering, North Carolina State University, Raleigh, North Carolina 27695, United States

Nicolas Morales-Gagnon – Department of Chemical & Biomolecular Engineering, North Carolina State University, Raleigh, North Carolina 27695, United States

Behnam Pourdeyhimi – Department of Textile Engineering, Chemistry, & Science, North Carolina State University, Raleigh, North Carolina 27695, United States

Frank Scholle – Department of Biological Sciences and Center for Advanced Virus Experimentation, North Carolina State University, Raleigh, North Carolina 27695, United States

Complete contact information is available at: https://pubs.acs.org/10.1021/acsami.0c16953

Notes

The authors declare no competing financial interest.

ACKNOWLEDGMENTS

This work was supported by the NC State Nonwovens Institute, Halyard Health, and the National Science Foundation (CNS-1844766 and IIP-2014753). Part of this study was performed in the North Carolina State University Analytical Instrumentation Facility (AIF), which is supported by the State of North Carolina and the National Science Foundation (ECCS-1542015). The AIF is a member of the North Carolina Research Triangle Nanotechnology Network (RTNN), a site in the National Nanotechnology Coordinated Infrastructure (NNCI).

REFERENCES

- (1) Scott, R. D., II The Direct Medical Costs of Healthcare-Associated Infections in U.S. Hospitals and the Benefits of Prevention; Centers for Disease Control and Prevention: Atlanta, 2009. www.cdc.gov/hai/pdfs/hai/scott_costpaper.pdf.
- (2) Neely, A. N.; Maley, M. P. Survival of Enterococci and Staphylococci on Hospital Fabrics and Plastic. *J. Clin. Microbiol.* **2000**, 38, 724–726.
- (3) Weber, D. J.; Rutala, W. A.; Miller, M. B.; Huslage, K.; Sickbert-Bennett, E. Role of Hospital Surfaces in the Transmission of Emerging Health Care-Associated Pathogens: Norovirus, Clostridium

- difficile, and Acinetobacter Species. Am. J. Infect. Control 2010, 38, S25-S33.
- (4) Baker, S.; Thomson, N.; Weill, F.-X.; Holt, K. E. Genomic Insights into the Emergence and Spread of Antimicrobial—Resistant Bacterial Pathogens. *Science* **2018**, *360*, 733—738.
- (5) Scutti, S. Unusual Forms of 'Nightmare' Antibiotic-Resistant Bacteria Detected in 27 States. *CNN Health*, April 4, 2018. https://www.cnn.com/2018/04/03/health/nightmare-bacteria-cdc-vital-signs/index.html.
- (6) Centers for Disease Control and Prevention. Antibiotic Resistance Threats in the United States. Department of Health and Human Services, CDC: Atlanta, GA, 2019. https://www.cdc.gov/drugresistance/pdf/threats-report/2019-ar-threats-report-508.pdf.
- (7) O'Neill, J. Tackling Drug-Resistant Infections Globally: Final Report and Recommendations; Review on Antimicrobial Resistance: London, 2016 (amr-review.org).
- (8) Reed, C.; Chaves, S. S.; Daily Kirley, P.; Emerson, R.; Aragon, D.; Hancock, E. B.; Butler, L.; Baumbach, J.; Hollick, G.; Bennett, N. M.; Laidler, M. R.; Thomas, A.; Meltzer, M. I.; Finelli, L. Estimating Influenza Disease Burden from Population-Based Surveillance Data in the United States. *PLoS One* **2015**, *10*, No. e0118369.
- (9) Biggs, H. M.; Lu, X.; Dettinger, L.; Sakthivel, S.; Watson, J. T.; Boktor, S. W. Adenovirus-Associated Influenza-Like Illness among College Students, Pennsylvania, USA. *Emerging Infect. Dis.* **2018**, 24, 2117–2119.
- (10) Chowell, G.; Abdirizak, F.; Lee, S.; Lee, J.; Jung, E.; Nishiura, H.; Viboud, C. Transmission Characteristics of MERS and SARS in the Healthcare Setting: A Comparative Study. *BMC Med.* **2015**, *13*, 210
- (11) Otter, J. A.; French, G. L. Survival of Nosocomial Bacteria and Spores on Surfaces and Inactivation by Hydrogen Peroxide Vapor. *J. Clin. Microbiol.* **2009**, 47, 205.
- (12) Hijnen, W. A. M.; Beerendonk, E. F.; Medema, G. J. Inactivation Credit of UV Radiation for Viruses, Bacteria and Protozoan (Oo)Cysts in Water: A Review. *Water Res.* **2006**, *40*, 3–22.
- (13) Richter, A. P.; Brown, J. S.; Bharti, B.; Wang, A.; Gangwal, S.; Houck, K.; Cohen Hubal, E. A.; Paunov, V. N.; Stoyanov, S. D.; Velev, O. D. An Environmentally Benign Antimicrobial Nanoparticle Based on a Silver-Infused Lignin Core. *Nat. Nanotechnol.* **2015**, *10*, 817–823.
- (14) Cioffi, N.; Torsi, L.; Ditaranto, N.; Tantillo, G.; Ghibelli, L.; Sabbatini, L.; Bleve-Zacheo, T.; D'Alessio, M.; Zambonin, P. G.; Traversa, E. Copper Nanoparticle/Polymer Composites with Antifungal and Bacteriostatic Properties. *Chem. Mater.* **2005**, *17*, 5255–5262
- (15) Kubacka, A.; Diez, M. S.; Rojo, D.; Bargiela, R.; Ciordia, S.; Zapico, I.; Albar, J. P.; Barbas, C.; Martins dos Santos, V. A. P.; Fernández-García, M.; Ferrer, M. Understanding the Antimicrobial Mechanism of TiO₂-Based Nanocomposite Films in a Pathogenic Bacterium. *Sci. Rep.* **2015**, *4*, No. 4134.
- (16) Jiao, Y.; Niu, L.; Ma, S.; Li, J.; Tay, F. R.; Chen, J. Quaternary Ammonium-Based Biomedical Materials: State-of-the-Art, Toxicological Aspects and Antimicrobial Resistance. *Prog. Polym. Sci.* **2017**, *71*, 53–90.
- (17) Zhu, D.; Cheng, H.; Li, J.; Zhang, W.; Shen, Y.; Chen, S.; Ge, Z.; Chen, S. Enhanced Water-Solubility and Antibacterial Activity of Novel Chitosan Derivatives Modified with Quaternary Phosphonium Salt. *Mater. Sci. Eng., C* **2016**, *61*, 79–84.
- (18) Harrison, J. J.; Ceri, H.; Turner, R. J. Multimetal Resistance and Tolerance in Microbial Biofilms. *Nat. Rev. Microbiol.* **2007**, *5*, 928–938
- (19) Stensberg, M. C.; Wei, Q.; McLamore, E. S.; Porterfield, D. M.; Wei, A.; Sepúlveda, M. S. Toxicological Studies on Silver Nanoparticles: Challenges and Opportunities in Assessment, Monitoring and Imaging. *Nanomedicine* **2011**, *6*, 879–898.
- (20) Hora, P. I.; Pati, S. G.; McNamara, P. J.; Arnold, W. A. Increased Use of Quaternary Ammonium Compounds during the SARS-CoV-2 Pandemic and Beyond: Consideration of Environmental Implications. *Environ. Sci. Technol. Lett.* **2020**, *7*, 622–631.

- (21) Qiao, Y.; Yang, C.; Coady, D. J.; Ong, Z. Y.; Hedrick, J. L.; Yang, Y.-Y. Highly Dynamic Biodegradable Micelles Capable of Lysing Gram-Positive and Gram-Negative Bacterial Membrane. *Biomaterials* **2012**, *33*, 1146–1153.
- (22) Peddinti, B. S. T.; Scholle, F.; Vargas, M. G.; Smith, S. D.; Ghiladi, R. A.; Spontak, R. J. Inherently Self-Sterilizing Charged Multiblock Polymers that Kill Drug-Resistant Microbes in Minutes. *Mater. Horiz.* **2019**, *6*, 2056–2062.
- (23) Peddinti, B. S. T.; Downs, S. N.; Yan, J.; Smith, S. D.; Ghiladi, R. A.; Mhetar, V.; Tocchetto, R.; Griffiths, A.; Scholle, F.; Spontak, R. J. Rapid and Repetitive Inactivation of SARS-CoV-2 and Human Coronavirus on Self-Disinfecting Anionic Polymers, submitted for publication.
- (24) Coronavirus Resource Center, Johns Hopkins University & Medicine, 2020. https://coronavirus.jhu.edu/map.html.
- (25) Carpenter, B. L.; Scholle, F.; Sadeghifar, H.; Francis, A. J.; Boltersdorf, J.; Weare, W. W.; Argyropoulos, D. S.; Maggard, P. A.; Ghiladi, R. A. Synthesis, Characterization, and Antimicrobial Efficacy of Photomicrobicidal Cellulose Paper. *Biomacromolecules* **2015**, *16*, 2482–2492.
- (26) Alvarado, D. R.; Argyropoulos, D. S.; Scholle, F.; Peddinti, B. S. T.; Ghiladi, R. A. A Facile Strategy for Photoactive Nanocellulose-Based Antimicrobial Materials. *Green Chem.* **2019**, *21*, 3424–3435.
- (27) Stanley, S. L.; Scholle, F.; Zhu, J.; Lu, Y.; Zhang, X.; Situ, X.; Ghiladi, R. A. Photosensitizer-Embedded Polyacrylonitrile Nanofibers as Antimicrobial Non-Woven Textile. *Nanomaterials* **2016**, *6*, 77.
- (28) Wainwright, M.; Maisch, T.; Nonell, S.; Plaetzer, K.; Almeida, A.; Tegos, G. P.; Hamblin, M. R. Photoantimicrobials-Are We Afraid of the Light? *Lancet Infect. Dis.* **2017**, *17*, No. e49.
- (29) Bartusik, D.; Aebisher, D.; Lyons, A. M.; Greer, A. Bacterial Inactivation by a Singlet Oxygen Bubbler: Identifying Factors Controlling the Toxicity of ¹O₂ Bubbles. *Environ. Sci. Technol.* **2012**, 46, 12098–12104.
- (30) Peddinti, B. S. T.; Scholle, F.; Ghiladi, R. A.; Spontak, R. J. Photodynamic Polymers as Comprehensive Anti-Infective Materials: Staying Ahead of a Growing Global Threat. *ACS Appl. Mater. Interfaces* **2018**, *10*, 25955–25959.
- (31) Peddinti, B. S. T.; Scholle, F.; Ghiladi, R. A.; Spontak, R. J. Antimicrobial Thermoplastic Elastomers: Strategic Pathways for the Future of Broad-spectrum Anti-infective Materials. *TPE Int. Mag.* **2019**, *11*, 235.
- (32) Bai, H.; Sun, Y.; Xu, J.; Dong, W.; Liu, X. Rheological and Structural Characterization of HA/PVA-SbQ Composites Film-Forming Solutions and Resulting Films as Affected by UV Irradiation Time. *Carbohydr. Polym.* **2015**, *115*, 422–431.
- (33) Fedorova, N.; Pourdeyhimi, B. High Strength Nylon Microand Nanofiber Based Nonwovens via Spunbonding. *J. Appl. Polym. Sci.* **2007**, *104*, 3434–3442.
- (34) Corman, V. M.; Baldwin, H. J.; Tateno, A. F.; Zerbinati, R. M.; Annan, A.; Owusu, M.; Nkrumah, E. E.; Maganga, G. D.; Oppong, S.; Adu-Sarkodie, Y.; Vallo, P.; da Silva Filho, L. V. R. F.; Leroy, E. M.; Thiel, V.; van der Hoek, L.; Poon, L. L. M.; Tschapka, M.; Drosten, C.; Drexler, J. F. Evidence for an Ancestral Association of Human Coronavirus 229E with Bats. J. Virol. 2015, 89, 11858–11870.
- (35) Tallury, S. S.; Pourdeyhimi, B.; Pasquinelli, M. A.; Spontak, R. J. Physical Microfabrication of Shape-Memory Polymer Systems via Bicomponent Fiber Spinning. *Macromol. Rapid Commun.* **2016**, *37*, 1837–1843.
- (36) Spearman, C. The Method of 'Right and Wrong Cases' ('Constant Stimuli') without Gauss's Formulae. *Brit. J. Psychol.* **1908**, 2, 227–242.
- (37) Kärber, G. Beitrag Zur Kollektiven Behandlung Pharmakologischer Reihenversuche Naunyn-Schmiedebergs. *Arch. Exp. Path. Pharmak.* **1931**, *162*, 480–483.
- (38) Stryjewski, M. E.; Corey, G. R. Methicillin-Resistant *Staphylococcus aureus*: An Evolving Pathogen. *Clin. Infect. Dis.* **2014**, 58, S10–S19.
- (39) Gardete, S.; Tomasz, A. Mechanisms of Vancomycin Resistance in *Staphylococcus aureus*. *J. Clin. Invest.* **2014**, 124, 2836–2840.

- (40) Balli, E. P.; Venetis, C. A.; Miyakis, S. Systematic Review and Meta-Analysis of Linezolid versus Daptomycin for Treatment of Vancomycin-Resistant Enterococcal Bacteremia. *Antimicrob. Agents Chemother.* **2014**, *58*, 734–739.
- (41) Qureshi, Z. A.; Hittle, L. E.; O'Hara, J. A.; Rivera, J. I.; Syed, A.; Shields, R. K.; Pasculle, A. W.; Ernst, R. K.; Doi, Y. Colistin-Resistant *Acinetobacter baumannii*: Beyond Carbapenem Resistance. *Clin. Infect. Dis.* **2015**, *60*, 1295–1303.
- (42) Falagas, M. E.; Tansarli, G. S.; Karageorgopoulos, D. E.; Vardakas, K. Z. Deaths Attributable to Carbapenem-Resistant *Enterobacteriaceae* Infections. *Emerging Infect. Dis.* **2014**, *20*, 1170–1175.
- (43) Scutti, S. Second U.S. Patient had Antibiotic-Resistant Superbug Infection. *CNN Health*, July 12, 2016. https://www.cnn.com/2016/07/12/health/superbug-second-us-patient/.
- (44) Boucher, H. W.; Talbot, G. H.; Bradley, J. S.; Edwards, J. E.; Gilbert, D.; Rice, L. B.; Scheld, M.; Spellberg, B.; Bartlett, J. Bad Bugs, No Drugs: No ESKAPE! An Update from the Infectious Diseases Society of America. *Clin. Infect. Dis.* **2009**, *48*, 1–12.
- (45) Hassan, R.; Seelman, S.; Peralta, V.; Booth, H.; Tewell, M.; Melius, B.; Whitney, B.; Sexton, R.; Dwarka, A.; Vugia, D.; Vidanes, J.; Kiang, D.; Gonzales, E.; Dowell, N.; Olson, S. M.; Gladney, L. M.; Jhung, M. A.; Neil, K. P. A Multistate Outbreak of *E. coli* O157:H7 Infections Linked to Soy Nut Butter. *Pediatrics* **2019**, 144, No. e20183978.
- (46) Glowacki, E. M.; Glowacki, J. B.; Chung, A. D.; Wilcox, G. B. Reactions to Foodborne *Escherichia coli* Outbreaks: A Text-Mining Analysis of the Public's Response. *Am. J. Infect. Control* **2019**, 47, 1280–1282.
- (47) van Doremalen, N.; Bushmaker, T.; Morris, D. H.; Holbrook, M. G.; Gamble, A.; Williamson, B. N.; Tamin, A.; Harcourt, J. L.; Thornburg, N. J.; Gerber, S. I.; Lloyd-Smith, J. O.; de Wit, E.; Munster, V. J. Aerosol and Surface Stability of SARS-CoV-2 as Compared with SARS-CoV-1. N. Engl. J. Med. 2020, 382, 1564—1567.
- (48) Chin, A. W. H.; Chu, J. T. S.; Perera, M. R. A.; Hui, K. P. Y.; Yen, H.-L.; Chan, M. C. W.; Peiris, M.; Poon, L. L. M. Stability of SARS-CoV-2 in Different Environmental Conditions. *Lancet Microbe* **2020**, *1*, No. e10.
- (49) Ullah, S.; Ullah, A.; Lee, J.; Jeong, Y.; Hashmi, M.; Zhu, C.; Joo, K. I.; Cha, H. J.; Kim, I. S. Reusability Comparison of Melt-Blown vs Nanofiber Face Mask Filters for Use in the Coronavirus Pandemic. *ACS Appl. Nano Mater.* **2020**, *3*, 7231–7241.
- (50) Cai, J.; Sun, W.; Huang, J.; Gamber, M.; Wu, J.; He, G. Indirect Virus Transmission in Cluster of COVID-19 Cases, Wenzhou, China, 2020. *Emerging Infect. Dis.* **2020**, 26, 1343–1345.